

# Optimal Scheduling of Integrated Energy Systems in Low-carbon Communities Considering Flexibility of Resources and Segmental Control of Solid Oxide Fuel Cells

Mao Yang, Yuxin Wang, Jinxin Wang, Dongxu Liu, and Weihang Xu

**Abstract**—To address the strong thermoelectric coupling of the combined heat and power (CHP) units, the low utilization rate of energy storage, and the underexploitation of load-side resource flexibility in integrated energy systems (IESs), this paper proposes an optimal scheduling model of an IES in low-carbon communities considering flexibility of resources and the segmental control of solid oxide fuel cells (SOFCs). Firstly, by replacing the gas turbine (GT) in the CHP unit with an SOFC array to reduce carbon emissions and simultaneously weakening the thermoelectric coupling of the CHP unit, the segmental control method is used to control the SOFC array to improve the overall efficiency of the CHP unit. Secondly, coupled interactions among different types of energy storage equipments are mobilized through the integrated energy storage system to make full use of the remaining space in the heat and natural gas storage tanks. Finally, load-side flexible resources are utilized by considering transferable, substitutable, and heat loads, taking into account the thermal inertia of the building and categorizing rooms based on floors, orientations, and room area. Additionally, different user characteristics are characterized, and the flexible resources of building heating periods in northern cities in China are tapped in depth according to the actual factors. Compared with the traditional model, the optimal scheduling model proposed in this paper can reduce the wind abandonment rate and the carbon emission of community-integrated energy system (CIES) by 4.54% and 70.63%, respectively, and increase the utilization rate of heat and natural gas storage tanks by 12.34% and 30.52%, respectively, and lower the total cost by ¥2183.6 under the premise of ensuring user comfort during energy consumption, which promotes the economic and low-carbon operation of the CIES.

**Index Terms**—Optimal scheduling, flexible resource, wind abandonment, combined heat and power (CHP), low-carbon operation, solid oxide fuel cell, integrated energy system (IES).

## I. INTRODUCTION

WITH the introduction of the target “carbon emission peaking and carbon neutrality”, the renewable energy installations in China are increasing [1]. However, this trend highlights several problems in integrated energy systems (IESs) in terms of the sizeable thermoelectric coupling of the combined heat and power (CHP) units [2], the low utilization of energy storage [3], and the underexploitation of flexibility of load-side resources [4], which directly contributes to the wind abandonment, whereby a large amount of wind resources are not effectively utilized. Therefore, it is necessary to strengthen the technical transformation and optimization of CHP units, improve the utilization rate of energy storage, fully tap into load-side flexibility, realize the sustainable and efficient utilization of new energy sources, and contribute to the transformation and upgrade of the energy infrastructure of China.

In the context of the energy crisis and environmental protection, conventional CHP technology has become a vital energy utilization method [5]. Compared with conventional gas turbines (GTs), solid oxide fuel cells (SOFCs) have a higher electricthermal conversion efficiency, which can more fully utilize chemical energy of fuel, reduce energy waste, and improve energy efficiency [6]–[8]. Owing to their operation principles and application of unique materials, SOFCs produce less pollutant emissions during the electrochemical process, which are more environmentally friendly [9]. However, the SOFC-CHP plants using a single SOFC are not suitable for scenarios with high electrothermal power demands because of their power rating limitations, and few studies address the combined operation and control of multiple SOFCs.

Existing studies on how IESs consume wind power suggest that IESs should be equipped with energy storage, which can maximize wind power resources by storing wind power during high wind power output periods and releasing it during low wind power output periods. Reference [10] applies a battery energy storage system for load shaving and peak filling to establish an optimization model to maximize the net benefit. A battery energy storage system configuration method is proposed in [11]. In addition, a thermoelectric hybrid energy storage system is used to increase the wind power accommodation of IES [11]. Part of the IES is

Manuscript received: November 14, 2023; revised: February 29, 2024; accepted: July 4, 2024. Date of CrossCheck: July 4, 2024. Date of online publication: August 26, 2024.

This work was supported by the Industrial Technology R&D Program of Jilin Province (No. 2023C033-5).

This article is distributed under the terms of the Creative Commons Attribution 4.0 International License (<http://creativecommons.org/licenses/by/4.0/>).

M. Yang, Y. Wang (corresponding author), J. Wang, D. Liu, and W. Xu are with the Key Laboratory of Modern Power System Simulation and Control & Renewable Energy Technology, Ministry of Education, Northeast Electric Power University, Jilin 132012, China (e-mail: yangmao820@163.com; 754810542@qq.com; 1436705235@qq.com; 458162373@qq.com; 1150658067@qq.com).

DOI: 10.35833/MPCE.2023.000888



equipped with energy storage, but could not entirely consume wind power. There still exists the wind abandonment phenomenon, primarily due to the lack of storage capacity [12]. However, too much energy storage capacity leads to high investment costs and low utilization rates of energy storage, and few studies explore how to balance the relationship between storage capacity and utilization rates of energy storage.

For load-side flexible resources, three main types of demand response exist: price-based demand response, which is based on the impact of time-of-energy prices; incentive-based demand response, which is based on incentive compensation instruments; and substitution-based demand response, which is based on the substitution of energy consumption by customers due to differences in heterogeneous energy price signals [13]. Existing studies demonstrate the economic and low-carbon benefits of integrated demand response for IES operations [14]. Among them, the flexibility of heat load regulation is also a critical factor in changing the IES ability to consume wind power, and tapping the potential of heat load regulation plays a vital role in realizing the economic and low-carbon operation of IES.

The heat network storage and discharge characteristics and the thermal inertia of the heating area under a CHP system are analyzed in [15] to exploit the elastic change in heat load resources relative to internal and external temperatures, promoting the wind power accommodation of IES. Reference [16] demonstrates that an integrated demand response for electricity and heat based on time-of-use tariffs and heating comfort ambiguity balances the IES economics and low-carbon nature. Notably, few studies address the mining of flexibility of the community building architecture, which has the potential to be mined in most northern cities in China with a relatively high proportion of residential areas and long heating time [17]. Moreover, existing models of thermal inertia of buildings are more general and cannot accurately portray the different characteristics of buildings for typical urban community users.

In summary, this paper focuses on combining multiple SOFCs to form a SOFC/GT-CHP system. A segmental control method is proposed to improve the overall efficiency of the CHP units and weaken the thermoelectric coupling of the CHP units. At the same time, to improve the utilization rate of energy storage, the remaining space of heat and natural gas storage is used to improve the utilization rate of wind power. The primary focus of this paper is to analyze the load-side flexible resources in community buildings during heating period, accounting for the actual factors involved in buildings and analyzing load-side flexible resources in depth.

This paper proposes an optimal scheduling model of IES in low-carbon communities considering flexibility of resources and the segmental control of SOFC to promote the wind power consumption, realize the economic and low-carbon operation of the community-integrated energy system (CIES), and ensure the stable and efficient consumption of energy.

## II. ARCHITECTURE OF OPERATION OF CIES

Figure 1 shows the block diagram of the CIES. As shown in Fig. 1, a CIES consists of an upper energy network con-

taining power grid and natural gas network. Wind power is a renewable energy source, and coupling equipment includes an SOFC/GT-CHP system, a power-to-gas (P2G), a gas boiler (GB), and a ground-source heat pump (GSHP). Among these resources, the electricity grid and wind turbine provide electricity and natural gas supplies, respectively; the natural gas networks and P2G provide natural gas supplies; and the SOFC/GT-CHP system, GB, and GSHP provide heat supplies. The combined energy storage system (CESS) stores excess energy in the CIES, converts, and releases it when needed. The energy demand side contains electric, heat, and natural gas loads.

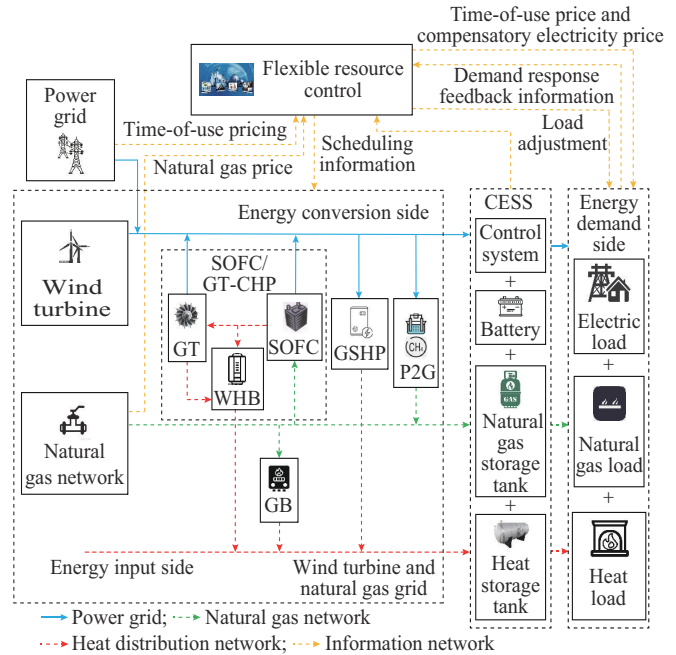


Fig. 1. Block diagram of CIES.

### A. SOFC/GT-CHP System

The operating principles of SOFC/GT-CHP system are shown in Fig. 2. The SOFC/GT-CHP system combines the power of an SOFC and a GT to improve the overall efficiency of CHP unit. The GT, which drives high-speed electric motor, can generate electricity from the exhaust waste heat generated by SOFCs at high temperature. Despite the leading role of the SOFC in power generation, the GT can be used as a backup device when needed.

### B. SOFC Array Control Strategy Based on Segmental Control Method

Considering that a single SOFC has a small generating power output, multiple SOFCs are required to produce energy simultaneously to meet high electric power demands. To control SOFCs, the simplest method is to start other SOFCs sequentially when a power shortage occurs. However, since the operating efficiency of an SOFC is related to the output power, the specific relationship of operating efficiency and output power is shown in Fig. 3. Thus, by controlling a single SOFC to maintain the optimal output power, the operating efficiency of each SOFC can be significantly improved, thus improving the overall efficiency.

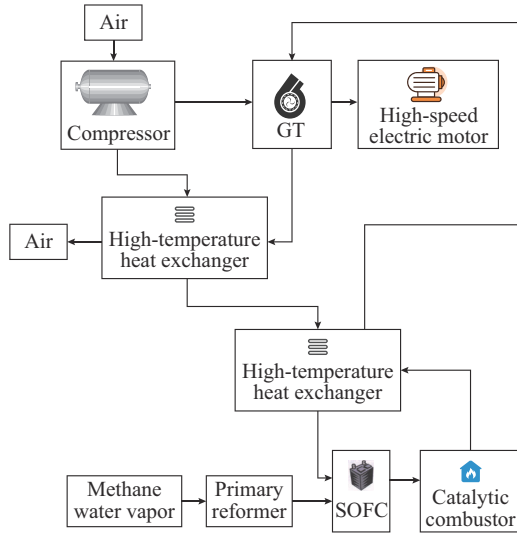


Fig. 2. Operating principles of SOFC/GT-CHP system.

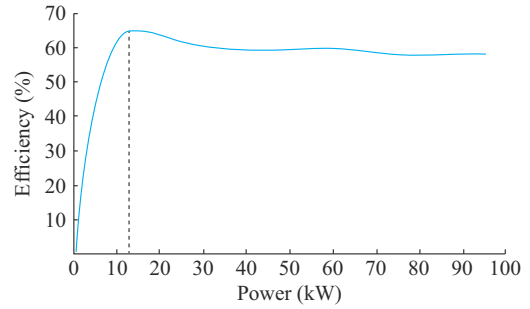


Fig. 3. Specific relationship of operating efficiency and output power.

As shown in Fig. 4, the segmental controller consists of a segmental control selector, a segmental selection switch,  $n$  SOFCs, and an actuator. Figure 5 shows the control diagram of SOFC based on segmental control. The specific process of the segmental control is as follows.

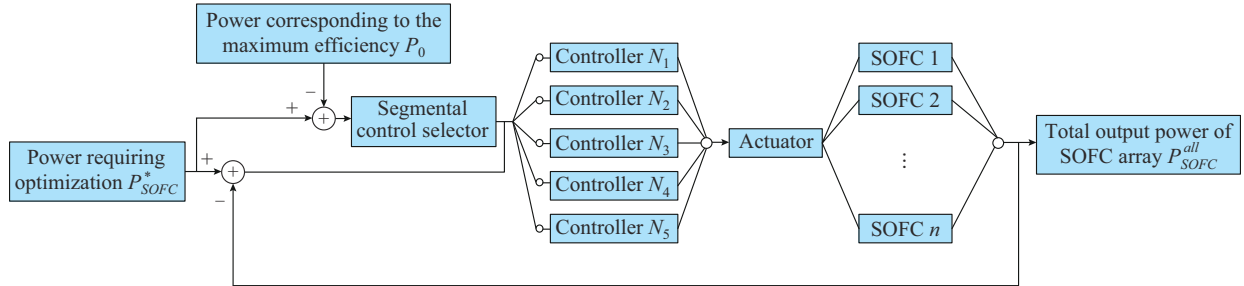


Fig. 4. Block diagram structure of segmental controller.

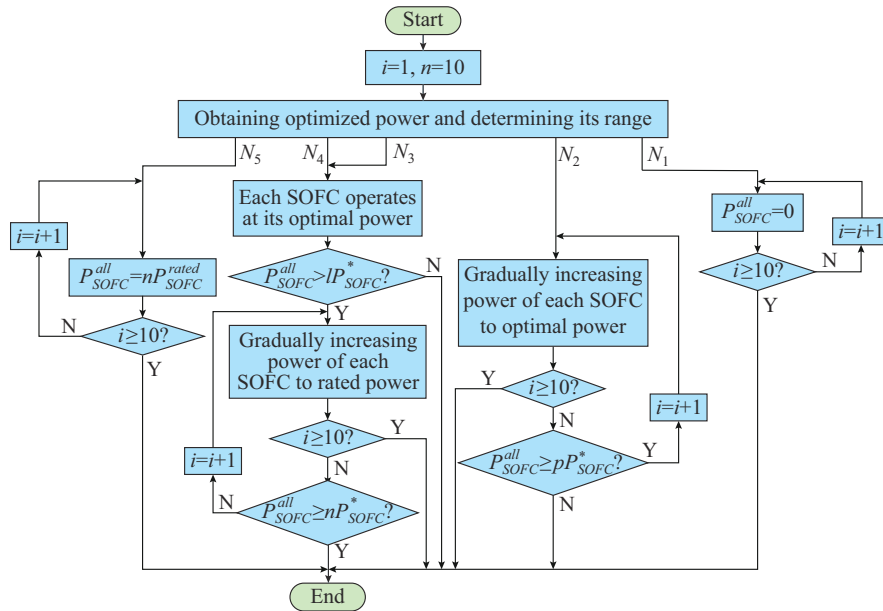


Fig. 5. Control diagram of SOFC based on segmental control.

*Step 1:* determine the output power of the SOFC array for each period according to the CIES scheduling results.

*Step 2:* determine the power output interval of the SOFC array.

*Step 3:* allocate the specific output power of each SOFC via *Step 1*, which is determined as follows: when  $P_{SOFC}^{all}$  is in power interval  $N_1$ , all the SOFCs do not operate; when  $P_{SOFC}^{all}$

is in power interval  $N_2$ , there are  $k$  SOFCs in the SOFC array with  $n$  SOFCs operating at the optimal output power, and the others do not operate; when  $P_{SOFC}^{all}$  is in power interval  $N_3$ , all the SOFCs in the SOFC array can operate at the optimal output power; when  $P_{SOFC}^{all}$  is in power interval  $N_4$ , all the SOFCs are operating, with  $l$  SOFCs operating at the rated power and the rest operating at the optimal output power.

er; and when  $P_{SOFC}^{all}$  is in power interval  $N_5$ , all the SOFCs are operating at the rated power.

According to the allocation above, the actuator execution is input to control each SOFC.

$$P_{SOFC}^{all} = \begin{cases} 0 & P_{SOFC}^{all} \in N_1 \\ kP_{SOFC}^o & k < n, P_{SOFC}^{all} \in N_2 \\ nP_{SOFC}^o & P_{SOFC}^{all} \in N_3 \\ lP_{SOFC}^{rated} + (n-l)P_{SOFC}^o & l < n, P_{SOFC}^{all} \in N_4 \\ nP_{SOFC}^{rated} & P_{SOFC}^{all} \in N_5 \end{cases} \quad (1)$$

where  $P_{SOFC}^o$  is the optimal output power of each SOFC; and  $P_{SOFC}^{rated}$  is the rated power of each SOFC.

### C. CESS

As a result of the increase in energy storage device for wind power accommodation, traditional energy storage device has limitations due to the limited capacity of the coupling device and the weak coupling link, thus reducing the utilization of the energy storage space.

The CESS includes control systems, batteries, heat storage tanks, and natural gas storage tanks, as well as storage tanks applicable for microconversion device. The microconversion device in the CESS does not operate when each energy storage state does not reach its peak value. When the battery reaches its limit and cannot hold the excess electric energy, the CESS can convert the excess electric energy to a microconversion device, which then convert the excess electric energy into natural gas and heat energy, where the remaining space in the natural gas and heat storage tanks is used to store natural gas and heat energy, respectively. As part of a CESS, the control system monitors and manages the conversion and storage processes among electric, thermal, and natural gas energy. The control system can intelligently optimize the way energy is converted and stored according to supply and demand, resulting in the highest possible efficiency of energy consumption.

The model representation is given as:

$$\begin{cases} P_{in}^{CESS} = P_{echa}^{CESS} + P_{hcha}^{CESS} + P_{pcha}^{CESS} \\ P_{out}^{CESS} = P_{edis}^{CESS} + P_{hdis}^{CESS} + P_{pdis}^{CESS} \\ P_p^{me2p} = P_e^{me2p} \lambda_{me2p} \\ P_h^{meh} = P_e^{meh} \lambda_{meh} \end{cases} \quad (2)$$

$$\begin{bmatrix} P_{edis}^{CESS} \\ P_{hdis}^{CESS} \\ P_{pdis}^{CESS} \end{bmatrix} = \begin{bmatrix} P_{echa}^{CESS} \\ P_{hcha}^{CESS} \\ P_{pcha}^{CESS} \end{bmatrix} + \begin{bmatrix} -1 & -1 & 0 \\ 0 & \lambda_{meh} & 0 \\ \lambda_{me2p} & 0 & 0 \end{bmatrix} \begin{bmatrix} P_e^{me2p} \\ P_e^{meh} \\ 0 \end{bmatrix} \quad (3)$$

where  $P_{in}^{CESS}$  and  $P_{out}^{CESS}$  are the input and output power of the CESS, respectively;  $P_{edis}^{CESS}$ ,  $P_{hdis}^{CESS}$ , and  $P_{pdis}^{CESS}$  are the discharging power, heat releasing power, and natural gas release power of the CESS, respectively;  $P_{echa}^{CESS}$ ,  $P_{hcha}^{CESS}$ , and  $P_{pcha}^{CESS}$  are the charging power, heating power, and inflation power of the CESS, respectively;  $P_e^{me2p}$  and  $P_p^{me2p}$  are the electric power consumed to charge the storage tanks with excess battery power and the natural gas power charged into the CESS, respectively;  $P_e^{meh}$  and  $P_h^{meh}$  are the electric power consumed to charge the heat storage tank with excess battery power and

the heating power as well as charged to the heat storage tank in the CESS, respectively; and  $\lambda_{me2p}$  and  $\lambda_{meh}$  are the operating efficiencies of the microconversion devices in the CESS.

To evaluate the efficiency of utilization of energy storage, this paper takes the capacity utilization rate of energy storage as an evaluation index.

$$\theta_{c,\ell} = \frac{C_{ac,\ell}}{C_{ra,\ell}} \times 100\% \quad (4)$$

where subscript  $\ell$  is the index of energy storage type;  $\theta_{c,\ell}$  is the capacity utilization rate;  $C_{ac,\ell}$  is the actual capacity; and  $C_{ra,\ell}$  is the total capacity.

## III. FLEXIBLE RESOURCES

### A. Flexible Heat Loads Considering Thermal Inertia of Building

Traditionally, centralized heating systems cause significant fluctuations in indoor temperature, which makes users uncomfortable. Within a building, distributed heating strategies are thermally inert, resulting in small fluctuations in indoor temperature. In this way, the stability and comfort of the indoor temperature can be improved, allowing for the use of operating strategies based on the temperature comfort zones of the users. Furthermore, it provides more room for the consumption of renewable energy.

#### 1) Level of Temperature Comfort Zone

Individuals have different indoor temperature comfort requirements during different time periods. Hence, their work and rest patterns are considered via a time-sharing model. On the basis of their indoor temperature comfort requirements, the time in a day can be classified into two time periods: daytime and nighttime [18]. Table I shows the indoor temperature comfort range of different time periods.

TABLE I  
INDOOR TEMPERATURE COMFORT RANGE OF DIFFERENT TIME PERIODS

Time period	Lower comfort limit (°C)	Upper comfort limit (°C)
07:00-22:00	20	24
22:00-07:00	17	21

#### 2) Equivalent Model of Room Temperature Variability Process

The temperature variability process in the building is determined by both the heating power of the electric heating device and the outdoor temperature. The schematic of the equivalent model of room temperature variability process shown in Fig. 6 can approximate the room temperature variability process [19]. The set of total parameter ordinary differential equations describing the room temperature change process is given as:

$$\begin{cases} C_{in} \frac{d\theta_{in}(t)}{dt} = P_{heat}(t) - \frac{\theta_{in}(t) - \theta_{wall}(t)}{R_1} \\ C_{wall} \frac{d\theta_{wall}(t)}{dt} = \frac{\theta_{in}(t) - \theta_{wall}(t)}{R_1} - \frac{\theta_{wall}(t) - \theta_{out}(t)}{R_2} \end{cases} \quad (5)$$

where  $C_{in}$  and  $C_{wall}$  are the equivalent heat capacity of the in-



demand relationship is tense, economic means should be provided to compensate for the user adjustments in hours, alleviating the imbalance between the supply and demand while also ensuring the stability of the IES. Load shifting from one period to another period can have a peak-shaving and valley-filling effect on the load curve. Although the total amount shifted remains the same throughout the cycle, it can affect user comfort. Therefore, there is a comfort cost.

$$\begin{cases} P_{i,load}^{ex}(t) = P_{i,load}^{ex0}(t) + \Delta P_{i,load}^{ex}(t) \\ \Delta P_{i,load}^{ex}(t) = S_i^{exin}(t)P_{i,load}^{exin}(t) - S_i^{exout}(t)P_{i,load}^{exout}(t) \\ S_i^{exin}(t) + S_i^{exout}(t) \leq 1 \\ \sum_{t=1}^T \Delta P_{i,load}^{ex}(t) = 0 \\ |\Delta P_{i,load}^{ex}| \leq \Delta P_{i,load}^{ex,max} \end{cases} \quad (8)$$

where  $P_{i,load}^{ex0}(t)$  is the predicted value of the load during period  $t$ ;  $P_{i,load}^{ex}(t)$  is the load after shifting during period  $t$ ;  $S_i^{exin}$  and  $S_i^{exout}$  are the 0-1 variables for load shifting during period  $t$  ( $S_i^{exin}=1$  denotes transfer in,  $S_i^{exout}=1$  denotes transfer out, and  $S_i^{exin}=S_i^{exout}=0$  denote no load shifting); and  $\Delta P_{i,load}^{ex,max}$  and  $\Delta P_{i,load}^{ex,min}$  are the upper and lower transfer limits, respectively.

#### IV. OBJECTIVE FUNCTION AND CONSTRAINTS

##### A. Objective Function

This paper aims to minimize the total cost of the CIES, which includes energy purchasing costs  $C_p$  from the primary power grid and natural gas network, carbon trading expenses  $C_{CO_2}$ , comfort compensation costs  $C_{COM}$ , and wind abandonment penalty costs  $C_w$ .

$$\min C = \min(C_p + C_{CO_2} + C_{COM} + C_w) \quad (9)$$

where  $C$  is the total cost of the CIES.

##### 1) Energy Purchasing Costs

$$C_p = \sum_{t=1}^{24} (P_{e,p}(t)c_e(t) + P_{p,p}(t)c_p(t)) \quad (10)$$

where  $P_{e,p}(t)$  is the amount of electricity purchased from the main power grid during period  $t$ ;  $P_{p,p}(t)$  is the amount of natural gas purchased from the main natural gas network during period  $t$ ; and  $c_e(t)$  and  $c_p(t)$  are the unit prices of purchased electricity and natural gas during period  $t$ , respectively.

##### 2) Carbon Trading Expenses

The actual carbon emissions for the electricity and heat supply of the CIES are determined via the following equations.

$$E_{IES} = \sum_{t=1}^T (a_1 + b_1 P_{e,p}(t) + c_1 P_{e,p}^2(t) + a_2 + b_2 P_{p,p}(t) + c_2 P_{p,p}^2(t)) \quad (11)$$

$$P_{pvr}(t) = P_{p,GB}(t)\eta_{GB} \quad (12)$$

where  $E_{IES}$  is the actual carbon emission of the CIES;  $a_1$ ,  $b_1$ , and  $c_1$  are the carbon emission calculation coefficients of electricity purchased from the main power grid;  $a_2$ ,  $b_2$ , and  $c_2$  are the carbon emission coefficients of heating;  $P_{p,GB}(t)$  is the input power of the GB during period  $t$ ; and  $\eta_{GB}$  is the en-

ergy conversion efficiency of the GB.

Multiple carbon credits purchase bands are delineated by the stepped carbon trading model. As the CIES needs to purchase more carbon credit allowances, the purchase price of the corresponding band is higher, thus limiting the output of the high-emission device [6]. The modified carbon trading model is given as:

$$C_{CO_2} = \begin{cases} aE_{IES} & E_{IES} \leq d \\ a(1+\omega)(E_{IES}-d) + ad & d < E_{IES} \leq 2d \\ a(1+2\omega)(E_{IES}-2d) + (2+\omega)ad & 2d < E_{IES} \leq 3d \\ a(1+3\omega)(E_{IES}-3d) + (3+3\omega)ad & 3d < E_{IES} \leq 4d \\ a(1+3\omega)(E_{IES}-4d) + (4+6\omega)ad & 4d < E_{IES} \end{cases} \quad (13)$$

where  $a$  is the base price for carbon trading;  $d$  is the interval length of carbon emissions of the CIES; and  $\omega$  is the rate of price increment.

##### 3) Comfort Compensation Costs

Substitutable loads can choose different energy supply methods to meet their energy demand simultaneously, and since they do not change the energy demand of the users, they do not incur comfort compensation costs. Heat loads that consider the thermal inertia of the building also satisfy the comfort zone of the user and therefore incur no comfort compensation costs.

$$C_{COM} = \sum_{t=1}^{24} \sum_{i=1}^3 \varepsilon |\Delta P_{i,load}^{ex}(t)| \quad (14)$$

where  $\varepsilon$  is the unit compensation coefficient for transferable loads.

##### 4) Wind Abandonment Penalty Costs

$$C_w = \varphi \sum_{t=1}^T P_{WP,cut}(t) \quad (15)$$

where  $\varphi$  is the penalty coefficient of the discarded wind power; and  $P_{WP,cut}(t)$  is the abandoned wind power.

#### B. Constraints

##### 1) Power Balance Constraints

$$\begin{cases} P_{e,p}(t) + P_{WP}(t) + P_{e,SOFC/GT-CHP}(t) = P_{e,Load}(t) + P_{e,P2G}(t) + P_{e,GSHP}(t) + P_{e,ES}(t) \\ P_{h,GB}(t) + P_{h,SOFC/GT-CHP}(t) + P_{h,GSHP}(t) = P_{h,Load}(t) + P_{h,ES}(t) \\ P_{g,p}(t) + P_{g,P2G}(t) = P_{g,Load}(t) + P_{g,SOFC/GT-CHP}(t) + P_{g,GB}(t) + P_{g,ES}(t) \end{cases} \quad (16)$$

where  $P_{WP}(t)$  is the actual wind power output during period  $t$ ;  $P_{i,Load}(t)$  is the overall load after the demand response during period  $t$ ;  $P_{e,P2G}(t)$  and  $P_{p,P2G}(t)$  are the electricity consumption and natural gas output of the P2G during period  $t$ , respectively;  $P_{p,GB}(t)$  and  $P_{h,GB}(t)$  are the natural gas consumption and heat output of the GB during period  $t$ , respectively;  $P_{e,SOFC/GT-CHP}(t)$ ,  $P_{h,SOFC/GT-CHP}(t)$ , and  $P_{g,SOFC/GT-CHP}(t)$  are the electricity output, heat power output, natural gas consumption of the SOFC/GT-CHP during period  $t$ , respectively; and  $P_{i,ES}(t)$  is the charging or discharging power of the CESS during period  $t$ .

## 2) Device Constraints

$$\begin{cases} \min P_i^k \leq P_i^k(t) \leq \max P_i^k \\ \min \Delta P_i^k(t) \leq P_i^k(t) - P_i^k(t-1) \leq \max \Delta P_i^k(t) \end{cases} \quad (17)$$

where  $\min P_i^k$  and  $\max P_i^k$  are the lower and upper limits of the output of the device during period  $t$ , respectively; and  $\min \Delta P_i^k(t)$  and  $\max \Delta P_i^k(t)$  are the lower and upper limits of the ramping power of the device during period  $t$ , respectively.

## 3) Wind Power Output Constraints

$$0 \leq P_{WP}(t) \leq P_{WPer}(t) \quad (18)$$

where  $P_{WP}(t)$  is the wind power output during period  $t$ ; and  $P_{WPer}(t)$  is the forecast of wind power output during period  $t$ .

## 4) Purchased Power Constraints

$$\begin{cases} \min P_{e,p} \leq P_{e,p}(t) \leq \max P_{e,p} \\ \min P_{p,p} \leq P_{p,p}(t) \leq \max P_{p,p} \end{cases} \quad (19)$$

where  $\min P_{e,p}$  and  $\max P_{e,p}$  are the lower and upper limits of the purchased power, respectively; and  $\min P_{p,p}$  and  $\max P_{p,p}$  are the lower and upper limits of the purchased natural gas, respectively.

## 5) CESS Constraints

CESS constraints include those related to charging and discharging power limitations of the CESS, those associated with energy conversion devices, energy state constraints, and energy storage capacity limitations.

$$\begin{cases} 0 \leq P_{i,cha}^{CESS}(t) \leq S_{i,cha}^{CESS}(t) P_{i,cha,max}^{CESS} \\ 0 \leq P_{i,dis}^{CESS}(t) \leq S_{i,dis}^{CESS}(t) P_{i,dis,max}^{CESS} \\ 0 \leq P_e^{me2p}(t) \leq S_e^{me2p} \min \{0.2S_e^{CESS}(t-1), P_{e,max}^{me2p}\} \\ 0 \leq P_e^{meh}(t) \leq S_e^{meh} \min \{0.2S_e^{CESS}(t-1), P_{e,max}^{meh}\} \\ S_e^{CESS}(t) = S_e^{CESS}(t-1) + \left( P_{e,cha}^{CESS}(t-1)\eta_{cha}^{CESS} - \frac{P_{e,dis}^{CESS}(t-1)}{\eta_{dis}^{CESS}} \right) \Delta t \\ S_h^{CESS}(t) = S_h^{CESS}(t-1) + \left[ (P_{h,cha}^{CESS}(t-1) + P_h^{meh}(t-1))\eta_{cha}^{CESS} - \frac{P_{h,dis}^{CESS}(t-1)}{\eta_{dis}^{CESS}} \right] \Delta t \\ S_p^{CESS}(t) = S_p^{CESS}(t-1) + \left[ (P_{p,cha}^{CESS}(t-1) + P_p^{me2p}(t-1))\eta_{cha}^{CESS} - \frac{P_{p,dis}^{CESS}(t-1)}{\eta_{dis}^{CESS}} \right] \Delta t \\ S_{i,cha}^{CESS} + S_{i,dis}^{CESS} \leq 1 \\ S_{e,com,e2p} + S_{p,dis}^{CESS} \leq 1 \\ S_{e,com,eh} + S_{h,dis}^{CESS} \leq 1 \\ S_i^{CESS}(1) = S_i^{CESS}(24) \\ P_{i,cae,min} \leq S_i^{CESS}(t)\Delta t \leq P_{i,cae,max} \end{cases} \quad (20)$$

where  $S_{i,cha}^{CESS}$  and  $S_{i,dis}^{CESS}$  are the indicators for CESS charging and discharging, respectively;  $P_{i,cha,max}^{CESS}$  and  $P_{i,dis,max}^{CESS}$  are the maximum charging and discharging power of the CESS, respectively;  $S_e^{me2p}$  and  $S_e^{meh}$  are the indicators of converting electricity to natural gas and electricity to heat, respectively;

$P_{e,max}^{me2p}$  and  $P_{e,max}^{meh}$  are the upper capacity limits of  $P_e^{me2p}$  and  $P_e^{meh}$ , respectively;  $S_i^{CESS}(t)$  is the energy state of each storage unit in the CESS during period  $t$ ;  $\eta_{cha}^{CESS}$  and  $\eta_{dis}^{CESS}$  are the charging and discharging efficiencies of the CESS, respectively; and  $P_{i,cae,min}$  and  $P_{i,cae,max}$  are the lower and upper capacity limits of each storage unit in the CESS, respectively.

## C. Simulation Environment

This paper uses a PC with an Intel Core i5 processor and 8 GB of RAM to build an optimal scheduling model via MATLAB simulation with the YALMIP toolkit. By using the GUROBI commercial solver, we can optimize the controllable variables while satisfying the constraints and obtain an optimal solution to the objective function.

## V. CASE STUDY

This paper takes a CIES in a residential area in the north-eastern of China as the research object, with  $N=300$  heating users, assuming that the structure of each building in the residential area is the same and the typical room classification is shown in Fig. 8. However, the area of each room in the same building is different. The experimental rooms are divided into three layers and five categories according to the floors, orientations, and room areas. The parameters of typical room construction are shown in Appendix A Table AI. The parameter fitting results of the typical room are in Appendix A Table AII. The unit comfort compensation cost of load shifting and substitution is 0.1 ¥/kWh, the unit abandoned wind penalty cost is 0.07 ¥/kWh, the growth rate of the step carbon trading price is 25%, the carbon base price is 0.252 ¥/kg, the transferable and alternative loads of electricity account for 10% of the total load, and the transferable and alternative loads of heat and natural gas account for 5% of the total load. The day-ahead forecast curves of loads and wind power are shown in Appendix A Fig. A1.

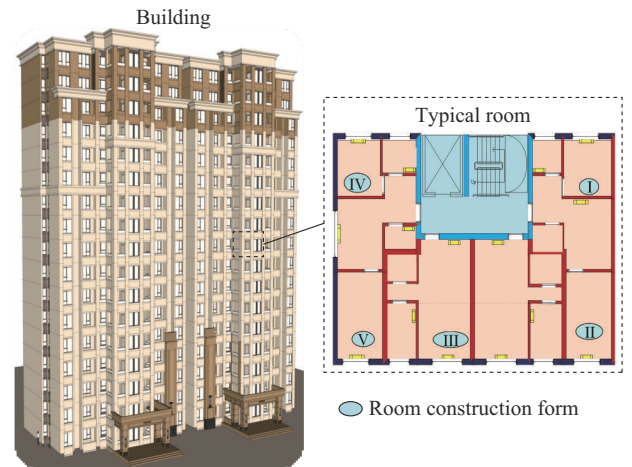


Fig. 8. Typical room classification.

In this paper, five different scenarios are investigated to evaluate the performance of the CIES, and the information of the five scenarios is shown in Table II. Scenario 1 is the conventional method, which includes a conventional GT-CHP.

TABLE II  
INFORMATION OF FIVE SCENARIOS

Scenario No.	Conventional GT-CHP	SOFC/GT-CHP simple control	SOFC/GT-CHP segmental control	Load-side flexible resource	CESS
1	√	×	×	×	×
2	×	√	×	×	×
3	×	×	√	×	×
4	×	×	√	√	×
5	×	×	√	√	√

### A. Comparative Analysis of Two CHP Systems

To analyze the advantages of the SOFC/GT-CHP over conventional GT-CHP, this paper compares various scenarios. Compared with the previous analysis, the SOFC/GT-CHP has the characteristic of high efficiency and low-carbon operation. Figure 9 shows the comparison of carbon emissions between scenarios 1 and 2. According to Fig. 9, the SOFC/GT-CHP produces almost no carbon emissions during operation, especially during the period of high electricity prices.

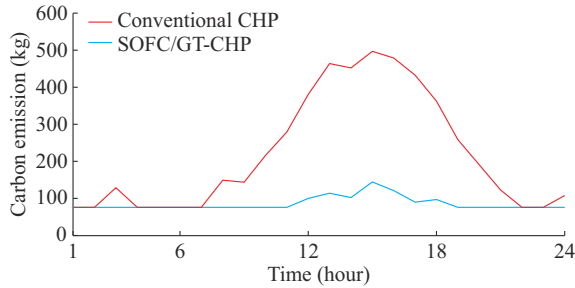


Fig. 9. Comparison of carbon emissions between scenarios 1 and 2.

SOFC/GT-CHP becomes the leading heating equipment, which significantly decreases carbon emissions of the CIES

with the increase of heating demand. Table III shows the costs and wind abandonment rates in various scenarios. According to Table III, after adopting the SOFC/GT-CHP, the total cost of the CIES is reduced by ¥1374.2, mainly due to the reduced carbon trading cost. Moreover, because the efficiency of SOFC/GT-CHP is higher than that of the conventional GT-CHP, to a certain extent, the conventional GT-CHP generated by the enormous heat load during the heating period is reduced, the thermoelectric coupling of the CHP is weakened, and some of the energy purchasing costs of the CIES are eliminated.

### B. Comparative Analysis of Two Kinds of Controls of SOFCs

According to Table III, when we compare the results under the SOFC/GT-CHP simple control (scenario 2) and the SOFC/GT-CHP segmental control (scenario 3), we can find that scenario 3 reduces the total costs by nearly ¥344 compared with scenario 2. The energy purchasing cost is reduced from ¥5368.1 to ¥5062.2. As a result of the segmental control in scenario 3, the SOFC array is highly flexible when faced with different power generation demands. Thus, the SOFC/GT-CHP can operate more efficiently, producing more electricity and heat at the same energy accommodation level while minimizing the energy purchasing costs.

TABLE III  
COSTS AND WIND ABANDONMENT RATES IN VARIOUS SCENARIOS

Scenario No.	Total cost (¥)	Energy purchasing cost (¥)	Carbon trading cost (¥)	Wind abandonment penalty cost (¥)	Comfort compensation cost (¥)	CESS investment cost/day (¥)	Wind curtailment rate (%)
1	7987.6	5728.4	1596.35	441.93	0	0	25.37
2	6613.4	5368.1	557.20	441.76	0	0	25.36
3	6269.2	5062.2	514.17	437.80	0	0	25.13
4	5904.7	4769.7	479.94	397.55	60.2	0	22.82
5	5804.0	4670.6	468.78	356.31	62.4	13.2	20.83

### C. Flexibility Analysis of Load-side Resources

#### 1) Load Shifting and Load Substitution

Scenario 4 considers load-side resources, which include transferable, substitutable, and heat loads. Figure 10 shows the load response in scenario 4. As observed from Fig. 10, for the transferable electric load, owing to the low wind power output during 11:00-20:00, the supply and demand relationship of electricity is tense. Moreover, since the SOFC/GT-CHP output reaches its capacity limit, the CIES incurs part of the energy purchasing cost. Thus, to reduce the energy purchasing cost of the CIES, the electric load can mainly transfer the load during the peak load period from 11:00 to

20:00 to the valley load period from 20:00 to 01:00. This measure can promote wind power accommodation, reduce the energy purchasing cost of the CIES, and also lower the heat load and natural gas load by adjusting the load distribution more reasonably. According to Fig. 11, for substitutable electric load, the equivalent natural gas price is lower than the equivalent electricity price during 00:00-08:00, on the basis of the equivalent electricity price calculated from the CIES. To maximize the user performance of the economy in terms of energy accommodation, natural gas and heat loads are substituted for electric loads as much as possible during this period. The same applies for other periods.

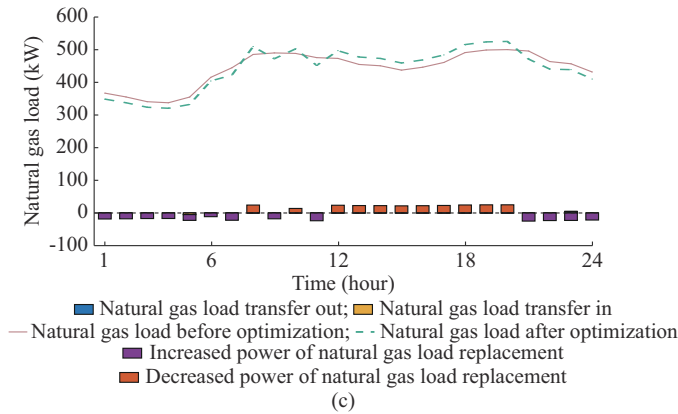
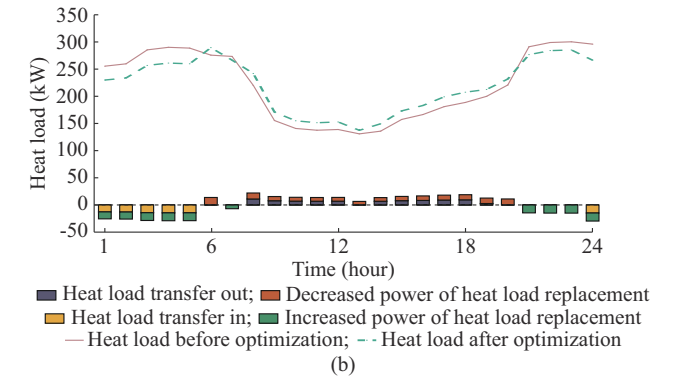
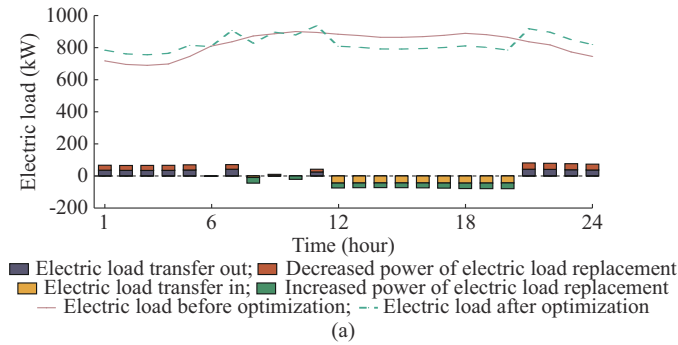


Fig. 10. Load response in scenario 4. (a) Electric load. (b) Heat load. (c) Natural gas load.

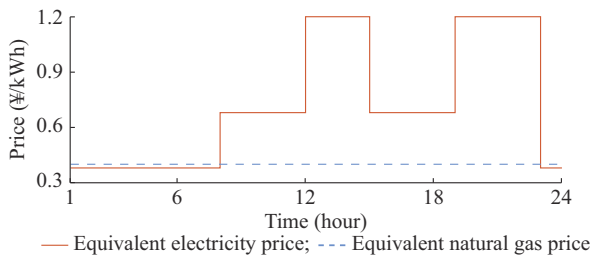


Fig. 11. Equivalent energy prices.

2) Flexible Heat Load Accounting for Thermal Inertia of Building

Temperature monitors are set up in the experimental rooms to analyze the changes in temperature and heat load in the building. The temperature curve of a random room in the community in the arithmetic example is shown in Fig. 12.

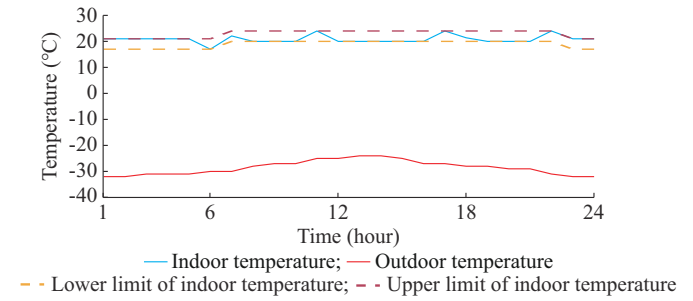


Fig. 12. Temperature curve of typical room

Figure 13 shows the power balance in scenario 4, which shows that as the wind power output increases between 22:00-24:00, the heat load is mainly met by the GSHP. To some extent, the change in the flexible heat load determines how much energy the CIES consumes. The flexible heat load should be increased as much as possible to dissipate excess wind power output during this period. Owing to the existence of the fuzzy intervals in the human body’s perception of temperature, the indoor temperature is increased. In this case, the room temperature does not affect the user comfort, so it reaches the upper comfort limit of the indoor temperature, at which point it stops increasing. In contrast, the flexible heat load increases significantly during 06:00-07:00. Owing to the change in the comfort zone, more heat is required indoors to meet the minimum temperature requirements. Afterward, to reduce the energy consumption and minimize the flexible heat load, the power increases during 10:00-11:00 when the equivalent electricity price is higher than the equivalent natural gas price. The CIES selects the more economical SOFC/GT-CHP to satisfy the heat load and recharges the batteries and heat storage tanks to cope with the period with high electricity price, and the CIES generates excess heat energy, which increases the indoor temperature. The CIES then cuts the flexible heat load to reduce the energy purchasing cost due to a gradual decrease in outdoor temperature. To reach the comfort zone, the CIES gradually increases the flexible heat load, and there is an air abandonment phenomenon during 20:00-21:00. Nevertheless, the indoor temperature does not change at this time because the climbing power of the GSHP is limited and the outdoor temperature decreases, which forces the GSHP to lift heat to counteract the change in outdoor temperature. The indoor temperature remains unchanged, causing the air abandonment phenomenon.

The scheduling process of flexible heat load participating in CIES is shown in Fig. 14. Combined with the analysis in Table III, scenario 4 reduces the total cost by ¥364.5 compared with scenario 3. It also reduces the wind abandonment rate by 2.31%, which shows that the flexibility of load-side resources considered in this paper can incentivize users to change their energy use habits to change the load profile. Therefore, wind power is accommodated more. Moreover, during the winter heating period, the CIES operator can control the overall heating for users, which can minimize part of the energy purchasing cost of the CIES while meeting the heat demands of the users, thus reducing the operating costs of the operator.

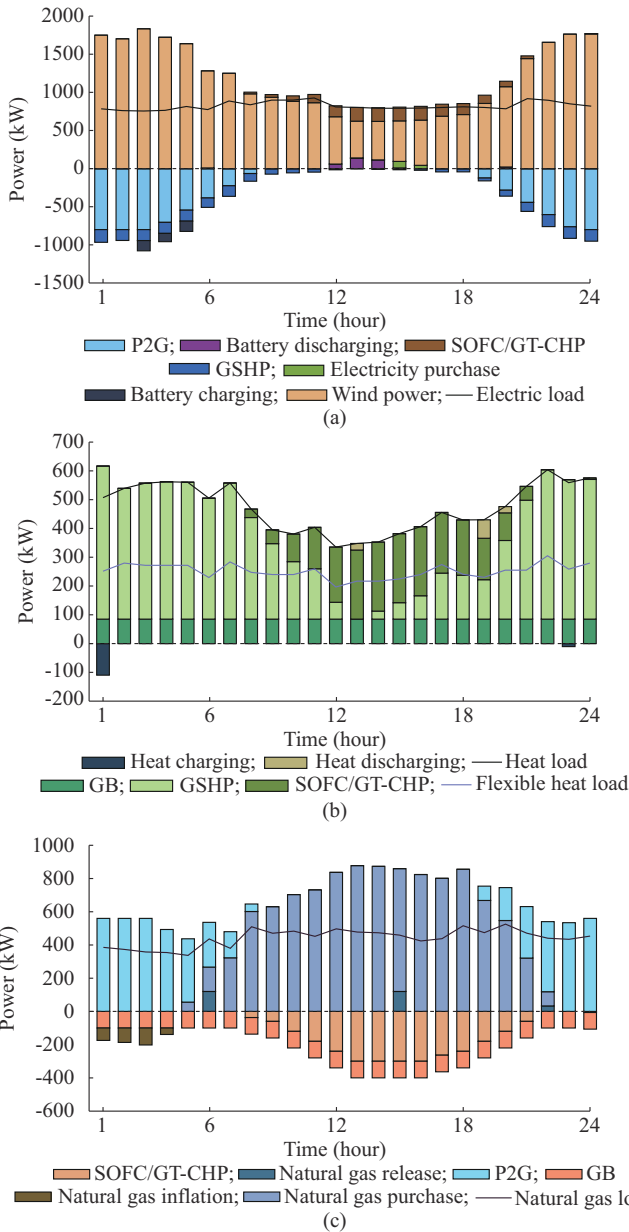


Fig. 13. Power balance in scenario 4. (a) Electric power balance. (b) Heat power balance. (c) Natural gas balance.

D. Comparative Analysis of CESS

Scenario 5 is the application of the CESS based on scenario 4. Figure 15 shows the energy storage comparison between scenarios 4 and 5. In scenario 4, the CIES may try to accommodate wind power due to the occurrence of the wind abandonment period. The electric energy storage space is fully utilized. In contrast, during the wind abandonment period, the demand for heat load is significant. Therefore, there is no excess heat to be stored in the heat storage tank, which results in a low utilization rate of the heat storage tank. The part of the space that needs to be fully utilized is for the scenarios in which wind power has a high utilization rate. As in scenario 4, the energy storage space in the natural gas storage tank needs to be fully utilized. In scenario 5, the charging and discharging pattern of the battery is unchanged in

the CESS because its space is fully utilized. With the control system and micro-conversion device in the CESS, wind power output can be converted into heat and natural gas energy during wind abandonment period, and be stored in the heat and natural gas storage tanks. The control system stores heat and natural gas energy into heat and natural gas storage tanks and releases it during the subsequent periods when heat and natural gas energy is needed.

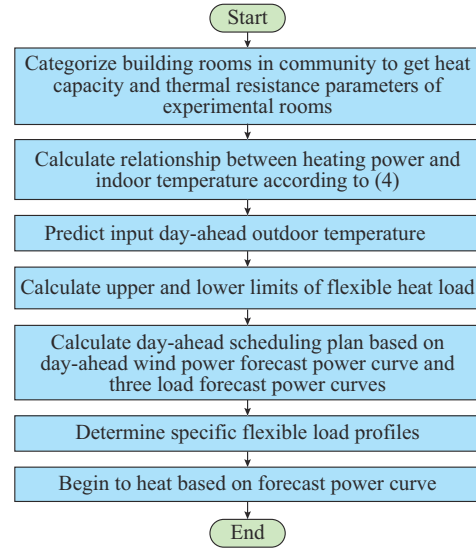


Fig. 14. Scheduling process of flexible heat load participating in CIES.

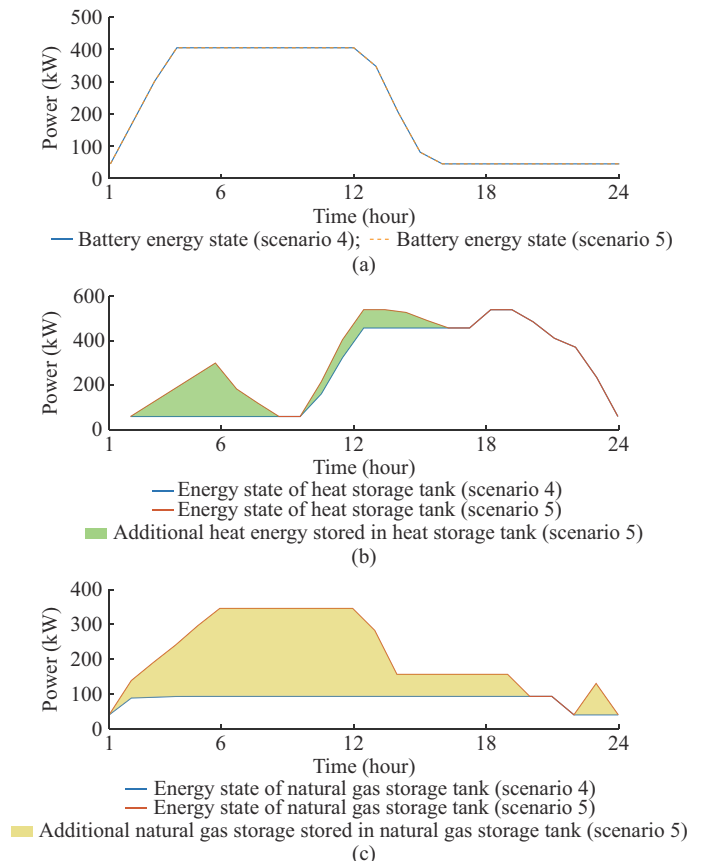


Fig. 15. Energy storage comparison between scenarios 4 and 5. (a) Battery energy state. (b) Energy state of heat storage tank. (c) Energy state of natural gas storage tank.

As shown in Fig. 15, since the amount of heat charged in the heat storage tank in the CESS is derived partly from the CIES heat flow and partly from the micro-conversion device in the CESS, the total amount of heat charged and released from the heat storage tank is increased in the overall scheduling process. The increased part is shown as the green area in Fig. 15, which is the additional heat energy stored in the heat storage tank. Similarly, the micro-conversion device increases the total charging and discharging power of the CESS. In scenario 5, compared with scenario 4, 12.34% more heat storage tanks are utilized, and 30.52% more natural gas storage tanks are utilized. Combined with the analysis of Table III, after the application of the CESS in the CIES, the total cost of the CIES is decreased by nearly ¥100. With the CESS, the wind abandonment rate is reduced by approximately 2%, so it can reduce the operating costs of the CIES and improve the system efficiency to a certain extent.

*E. Impact of Thermal Resistance and Thermal Capacitance of Room*

To explore the impact of different insulation materials on the total cost of the CIES, different thermal resistances and thermal capacitances are used in scenario 4 for a comparative analysis. In scenario 4, the thermal capacitance and thermal resistance are increased by 5% in turn. To analyze the effects of thermal capacitance and thermal resistance separately, the thermal capacitance is kept unchanged while the impacts of different thermal resistances are analyzed. Figure 16 shows the trends of total cost and abandonment rate under growth rate of different thermal resistances ( $R_1$  and  $R_2$  at the same rate at the same time as the growth rate).

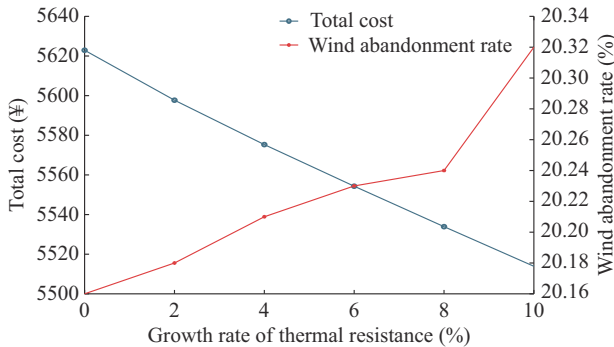


Fig. 16. Trends of total cost and abandonment rate under growth rate of different thermal resistances.

With the increase of the growth rate of the thermal resistance, the total cost of the CIES shows a downward trend. The main reason is that the physical meaning of the thermal resistance is the performance of the insulation. Therefore, the greater the thermal resistance of the room, the better the performance of the thermal insulation. When the indoor temperature is low, the heating device releases heat to warm the room. The better the thermal insulation, the slower the indoor heat transfer to the outdoors, i.e., the slower the heat loss, which is reflected on the energy supply side. Thus, the demand for heat energy is reduced. The energy demand of the CIES is further reduced, i.e., the energy purchasing cost

of the CIES is reduced. During high wind power output periods, the wind energy consumption is reduced, and the wind abandonment rate is increased. However, the reduction in the energy purchasing cost is more related to the increase in the wind abandonment penalty cost, so the total cost gradually decreases as the wind abandonment penalty cost increases.

Similarly, in the following analysis of the impact of different thermal capacities of the room on the operating cost of the CIES and the wind abandonment rate, the trends in total cost and wind abandonment rate under different thermal capacitances are shown in Fig. 17. The thermal capacity refers to the ability of the room to store heat energy, which depends on its mass, material, temperature, and other factors. The greater the thermal capacity of the room is, the more the heat which is needed to increase the indoor temperature. As the thermal capacity increases, the heat needed to increase the indoor temperature increases. Hence, the energy purchasing cost of the CIES is greater, and the amount of wind power accommodated during the wind abandonment period increases, resulting in a decrease in the wind abandonment rate. However, the higher unit energy purchasing cost results in an increase in the total cost of the CIES.

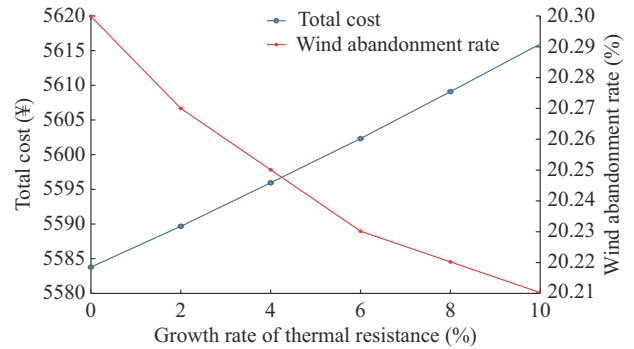


Fig. 17. Trends in total cost and wind abandonment rate under different room thermal resistances.

According to the above analysis, the parameters of the typical room have a particular impact on the economic operation of the CIES, so the thermal resistances and thermal capacitances are carefully considered in the selection of room insulation materials and CIES operation. This paper studies only a typical day in winter. Under high cooling demand on a typical summer day, distinct trends and their impacts become evident.

VI. CONCLUSION

This paper proposes an optimal scheduling model of an IES in low-carbon communities considering flexibility of resources and segmental control of SOFC, addressing the strong thermoelectric coupling of the CHP, the low utilization rate of energy storage, and underexploitation of flexibility of load-side resources. The conclusions are as follows.

1) When the SOFC/GT-CHP system is introduced, the CIES carbon trading cost is reduced by nearly ¥1020 relative to that of the conventional scenario. The SOFC array control strategy based on the segmental control method proposed in this paper improves the overall efficiency of the

CHP, weakens the thermoelectricity coupling of the CHP, and reduces the energy purchasing cost of the CIES by nearly ¥360.

2) The CESS applied in this paper effectively improves the utilization of the storage capacity in natural gas and heat storage tanks, stores electric energy that cannot be utilized owing to system constraints, reduces the total cost, and lowers the wind abandonment rate.

3) In this paper, transferable, substitutable, and heat loads are considered, and the thermal inertia of buildings is considered on the load side. Community buildings during the heating period in northern cities in China are explored in detail as flexible resources. Rooms are classified by comparing the floors, orientations, and room areas of buildings to characterize the differences in user characteristics, which effectively improves the utilization rate of wind power of the CIES without affecting the user comfort, benefits both the user and the CIES operator, and reduces the total operating costs of the CIES. The total operating cost of the CIES increases inversely with the thermal capacitance and thermal resistance when different room thermal capacities and room thermal resistances are compared.

#### APPENDIX A

TABLE AI  
PARAMETERS OF TYPICAL ROOM CONSTRUCTION

Floor	Form	Placement	Room size (m <sup>2</sup> )	Room volume (m <sup>3</sup> )	External wall area (m <sup>2</sup> )	External window area (m <sup>2</sup> )
Top	I	Shaded-middle	9.9	24.0	17.8	2.7
	II	Sunny-center 1	15.6	37.7	23.5	3.1
	III	Sunny-center 2	11.3	27.4	20.1	3.5
	IV	Shaded-side	10.1	24.4	25.4	2.7
	V	Sunny-side	15.6	37.7	35.1	3.1
Middle	I	Shaded-middle	9.9	24.0	7.9	2.7
	II	Sunny-center 1	15.6	37.7	7.9	3.1
	III	Sunny-center 2	11.3	27.4	8.8	3.5
	IV	Shaded-side	10.1	24.4	15.4	2.7
	V	Sunny-side	15.6	37.7	19.5	3.1
Ground	I	Shaded-middle	9.9	24.0	17.8	2.7
	II	Sunny-center 1	15.6	37.7	23.5	3.1
	III	Sunny-center 2	11.3	27.4	20.1	3.5
	IV	Shaded-side	10.1	24.4	25.4	2.7
	V	Sunny-side	15.6	37.7	35.1	3.1

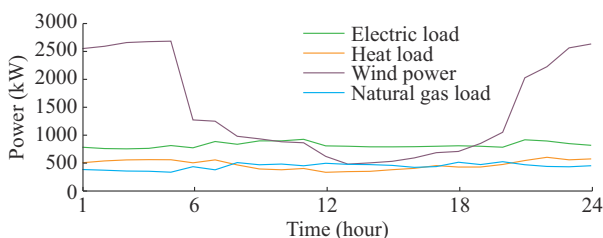


Fig. A1. Day-ahead forecast curves of loads and wind power.

TABLE AII  
PARAMETER FITTING RESULTS OF A TYPICAL ROOM

Form	Floor	$R_1$ (°C/W)	$R_2$ (°C/W)	$C_m$ (10 <sup>5</sup> J/°C)	$C_{wall}$ (10 <sup>5</sup> J/°C)
I	Top	0.0038	0.044	2.1	113.0
	Middle	0.0041	0.045	1.9	174.3
	Ground	0.0042	0.038	1.7	213.8
II	Top	0.0044	0.076	1.6	332.1
	Middle	0.0036	0.077	2.2	186.9
	Ground	0.0031	0.047	3.3	253.9
III	Top	0.0033	0.067	2.7	246.0
	Middle	0.0019	0.083	4.0	235.7
	Ground	0.0039	0.043	1.9	179.8
IV	Top	0.0037	0.052	2.6	185.8
	Middle	0.0041	0.047	2.2	177.3
	Ground	0.0023	0.028	4.0	220.2
V	Top	0.0038	0.032	2.0	207.1
	Middle	0.0036	0.034	3.0	371.0
	Ground	0.0022	0.022	2.2	620.6

#### REFERENCES

- [1] G. Chen, Y. Dong, Z. Liang *et al.*, "Analysis and reflection on high-quality development of new energy with chinese characteristics in energy transition," *Proceedings of the CSEE*, vol. 140, pp. 5493-5506, Aug. 2020.
- [2] X. Guo, S. Lou, Z. Chen *et al.*, "Stochastic optimal scheduling considering reserve characteristics of retrofitted combined heat and power plants," *International Journal of Electrical Power & Energy Systems*, vol. 140, p. 108051, Sept. 2022.
- [3] Y. Zhou, J. Wang, Y. Li *et al.*, "A collaborative management strategy for multi-objective optimization of sustainable distributed energy system considering cloud energy storage," *Energy*, vol. 280, p. 128183, Oct. 2023.
- [4] Y. Qiu, S. Lu, H. Lu *et al.*, "Flexibility of integrated energy system: basic connotation, mathematical model and research framework," *Automation of Electric Power Systems*, vol. 46, no. 18, pp. 16-43, Sept. 2022.
- [5] J. J. Fitzpatrick and R. Dunphy, "Comparison of the carbon footprints of combined heat and power (CHP) systems and boiler/grid for supplying process plant steam and electricity," *Chemical Engineering Science*, vol. 282, p. 119303, Dec. 2023.
- [6] J. Chen, Z. HU, J. Chen *et al.*, "Optimal dispatch of integrated energy system considering ladder-type carbon trading and flexible double response of supply and demand," *High Voltage Engineering*, vol. 47, pp. 3094-3106, Sept. 2022.
- [7] K. Abouemara, M. Shahbaz, G. McKay *et al.*, "The review of power generation from integrated biomass gasification and solid oxide fuel cells: current status and future directions," *Fuel*, vol. 360, p. 130511, Mar. 2024.
- [8] S. K. Effatpanah, H. R. Rahbari, M. H. Ahmadi *et al.*, "Green hydrogen production and utilization in a novel SOFC/GT-based zero-carbon cogeneration system: a thermodynamic evaluation," *Renewable Energy*, vol. 219, p. 119493, Dec. 2023.
- [9] M. Bakała, K. Martsinchyk, K. Motyliński *et al.*, "Numerical analysis of natural gas, hydrogen and ammonia fueled solid oxide fuel cell based micro cogeneration units with anodic gas recirculation," *International Journal of Hydrogen Energy*, vol. 52, pp. 952-964, Jan. 2024.
- [10] J. Cai, Q. Xu, X. Yuan *et al.*, "Configuration strategy of large-scale battery storage system orienting wind power consumption based on temporal scenarios," *High Voltage Engineering*, vol. 45, pp. 993-1001, Mar. 2019.
- [11] J. Li, Y. Fu, C. Li *et al.*, "Economic optimal configuration of hybrid energy storage system for improving wind power consumption," *Power System Technology*, vol. 44, no. 12, pp. 4547-4557, Dec. 2020.
- [12] W. Huang, D. Liu, S. Li *et al.*, "Two-level optimization of integrated energy system with P2G and demand response under dual carbon objective," *Electrical Measurement & Instrumentation*, vol. 59, pp. 8-

- 17, Nov. 2022.
- [13] Y. Cui, F. Guo, X. Fu *et al.*, "Source-load coordinated optimal dispatch of integrated energy system based on conversion of energy supply and use to promote wind power accommodation," *Power System Technology*, vol. 46, no. 4, pp.1437-1447, Apr. 2022.
- [14] P. Li, D. Wu, Y. Li *et al.*, "Optimal dispatch of multi-microgrids integrated energy system based on integrated demand response and stackelberg game," *Proceedings of the CSEE*, vol. 41, pp.1307-1321, Feb. 2021.
- [15] Z. Yi and Z. Li, "Combined heat and power dispatching strategy considering heat storage characteristics of heating network and thermal inertia in heating area," *Power System Technology*, vol. 42, no. 5, pp. 1378-1384, May 2018.
- [16] Y. Cui, C. Gu, X. Fu *et al.*, "Low-carbon economic dispatch of integrated energy system with carbon capture power plants considering generalized electric heating demand response," *Proceedings of the CSEE*, vol. 42, pp. 8431-8446, Dec. 2022.
- [17] Z. Liu. (2018, May). Research on the application of complementary heating system based on GSHP+ASHP+solar energy in northern towns. [Online]. Availbale: [https://kns.cnki.net/kcms2/article/abstract?v=upp0mjVwiKUvY2j\\_RCRbE35CqiGyV17ngyN18JttDckBfHcY-WF64gGVpGB1FMhkiLycVrGtIrTOeRWNVACSP7bFYrKt\\_ko56md0Z4n7\\_tPqCHPz4Rxxw6BUfY14FFFiFzVze6zFYynQ73ung51KmSUDMDE-GhBpR-jZfdi4fg5JclawaVVIIYq0U31yYFBMyqLCBfdPTQxK40=&uniplatform=NZKPT&language=CHS](https://kns.cnki.net/kcms2/article/abstract?v=upp0mjVwiKUvY2j_RCRbE35CqiGyV17ngyN18JttDckBfHcY-WF64gGVpGB1FMhkiLycVrGtIrTOeRWNVACSP7bFYrKt_ko56md0Z4n7_tPqCHPz4Rxxw6BUfY14FFFiFzVze6zFYynQ73ung51KmSUDMDE-GhBpR-jZfdi4fg5JclawaVVIIYq0U31yYFBMyqLCBfdPTQxK40=&uniplatform=NZKPT&language=CHS)
- [18] H. Liu, Y. Wang, J. Li *et al.*, "Coordinated heat and power dispatch of micro-energy network of countryside considering heat balance model of building and flexible indoor comfort constraints," *Automation of Electric Power Systems*, vol. 43, no. 10, pp. 50-58, May 2019.
- [19] H. Jia, Y. Lei, X. Jin *et al.*, "Collaborative optimization of building aggregation and integrated community energy system considering difference in insulation performance," *Automation of Electric Power Systems*, vol. 47, no. 24, pp.31-38, Dec. 2023.
- Mao Yang** received the M.S. degree in operation research and cybernetics from Jilin University, Changchun, China, in 2007, and the Ph.D. degree in control theory and control engineering from Jilin University, in 2010. He is currently the Vice Dean of the School of Electrical Engineering and a Professor at Northeast Electric Power University, Jilin, China. His research interests include renewable energy power forecasting and optimal scheduling of integrated energy system.
- Yuxin Wang** received the B.S. degree in electrical engineering from Northeast Electric Power University, Jilin, China, in 2022. He is currently pursuing the M.S. degree at Northeast Electric Power University. His research interest includes optimal scheduling of integrated energy system.
- Jinxin Wang** received the M.E. degree in electrical engineering from Northeast Electric Power University, Jilin, China, in 2020. He is currently working toward the Ph.D. degree at Northeast Electric Power University. His research interest includes optimal scheduling of microgrid.
- Dongxu Liu** received the B.S. degree in information and computational science from Northeast Electric Power University, Jilin, China, in 2019. He is currently pursuing the M.S. degree at Northeast Electric Power University. His research interest includes optimal scheduling of integrated energy system.
- Weihang Xu** received the B.S. degree in electrical engineering from Northeast Electric Power University, Jilin, China, in 2021. He is currently pursuing the M.S. degree at Northeast Electric Power University. His research interest includes wind power forecasting.